

An Improved E-Plane Waveguide Power Divider Design for 94GHz Dual-Pyramidal Horn Antenna

Xiaoyan Zhang^{1,2}, Yuting Chen^{1*}, Yan Xie^{1,3}, and Lingfeng Liu¹

¹ School of Information Engineering
East China Jiaotong University, Nanchang, 330013, China
xyzhang3129@ecjtu.jx.cn, *cytztgao@qq.com, 195915348@qq.com, lingfeng.liu@163.com

² State Key Laboratory of Millimeter Waves, Nanjing, 210096, China

³ Beibo (Xiamen) Intelligent Technology Co., Ltd., Xiamen, 361006, China

Abstract — In this paper, a waveguide power divider is proposed for a 94 GHz horn antenna. The entire structure was machined using 3D printing technology, and is comprised of two pyramidal horn antennas, a one to two E-plane waveguide power divider, three waveguide bends, and a flange. By introducing a wedge-shaped groove, two trapezium taper ports, and a $\lambda/2$ extension on the T-junction of the waveguide, we found improved impedance matching of the power divider, and the two output ports had the same phase. Our results show that the bandwidth of the antenna was 3.2% (3 GHz), its gain was higher than 21.2 dBi with an approximately 10° half power beam width at 94 GHz, and it could be applied to a precise location at close range (6 m to 10 m), which is suitable for automotive radar applications.

Index Terms — 3D printing, automotive, one dimensional range profile, pyramidal horn, waveguide power divider.

I. INTRODUCTION

As a key element in an automotive radar system, anti-collision radar usually works using a millimeter wave band, such as 24 GHz [1] or 77 GHz [2, 3]. These two bands are usually used for Long Range Radar (LRR) and Medium Range Radar (MRR). At a short range, 94 GHz radar is commonly used because it has a small wavelength (3.19 mm) that can detect small obstacles and locate targets more accurately [4, 5].

The antennas for the 94 GHz radar are mainly patch antennas [6], substrate integrated waveguide (SIW) antennas [7, 8], and horn antennas [9, 10]. Generally, in order to achieve a high gain, the patch antenna and the SIW antenna have to be made into an array, inevitably producing a large physical size. In [6] and [7], the maximum size of two antenna arrays was more than 20 times and 30 times that of their respective in order to maintain a gain greater than 20 dBi. However, other

research using horn antenna aperture less than 10 times the wavelength generated more than 20 dBi gain [8, 9]. Traditionally, horn antenna structures include an E-plane sectorial horn, a H-plane sectorial horn [10], a conical horn [11], and a pyramidal horn [12]. Among them, the pyramidal horn antenna can achieve a higher gain with the same aperture size. According to design requirements, different E- and H-plane beams can be obtained by changing the aperture size of the pyramidal horn antenna.

The feed of the horn antenna is mainly a coaxial feed [13], used only for feeding a single horn; a waveguide slot feed [14], which is more suitable for feeding a large waveguide slot array with more than four horns; a waveguide power divider feed [15], which can feed multiple horns and has the advantages of a smaller volume and less transmission loss in high frequencies than the waveguide slot feed. Based on the above general characteristics, the waveguide power divider should be a suitable choice for the 94 GHz horn antenna feed.

The general waveguide power divider is improved on the basis of the traditional E- or H-plane T junction waveguide, which has a discontinuous structure leading to strong reflection and attenuation of electromagnetic waves [16]. In order to reduce the return loss of waveguide power dividers, some structures such as a step impedance transformer [17] and a step-shaped groove [18] have been added in the T junctions to counteract their discontinuity. However, the S_{11} of the power dividers was only reduced to about -25 dB at 94 GHz [19]. Importantly, the two output ports of the divider have opposite phases [20]. In this paper, we propose an E-plane T junction waveguide power divider for a 94 GHz dual-pyramidal horn antenna. A wedge-shaped groove and two trapezium taper ports were added to improve impedance matching. Additionally, a length of $\lambda/2$ was extended to one trapezium taper port to allow the two output ports to share the same phase.

This paper is arranged as follows. In Section II, the configuration of the proposed antenna and the waveguide power divider are described in detail. In Section III, we present our results. In Section IV, a conclusion is made.

II. ANTENNA CONFIGURATION AND DESIGN

A. Waveguide power divider design

The proposed E-plane waveguide power divider is shown in Fig. 1. This was designed based on a T junction waveguide. As Fig. 1 (a) shows, a wedge-shaped groove and the trapezium taper ports were added on the T junctions. The trapezoidal sections have a smaller waveguide height “ n ” than WR-10 at the T-junction and then taper to the standard WR-10 height at the ports. Each port is a standard rectangular waveguide WR-10. Originally, the two output ports were on both sides, so two 90° bends are added to put the port2 and port3 in the same side as shown in Fig. 1 (b). In addition, a length of $\lambda_g/2$ was extended to the right trapezium taper port. Here λ_g is the guided wavelength, which can be calculated by:

$$\lambda_g = \lambda_0 / \left[1 - \left(\frac{\lambda_0}{\lambda_c} \right)^2 \right]^{1/2}, \quad (1)$$

where, λ_0 and λ_c are the operating wavelength and the cutoff wavelength, respectively.

To investigate the efficiency of the proposed T junction in Fig. 1 (a), the simulated S_{11} was compared in four cases (as shown in Table 1) and, as shown in Fig. 2 (a), the wedge-shaped groove and the trapezium taper port reduce the electromagnetic reflection of the waveguide. Among these characteristics, the introduction of the wedge-shaped groove led to the greatest improvement in impedance matching. Obviously, our proposed T junction has a minimum S_{11} in the whole working frequency band. Thus, the proposed design has better impedance matching than the other three cases.

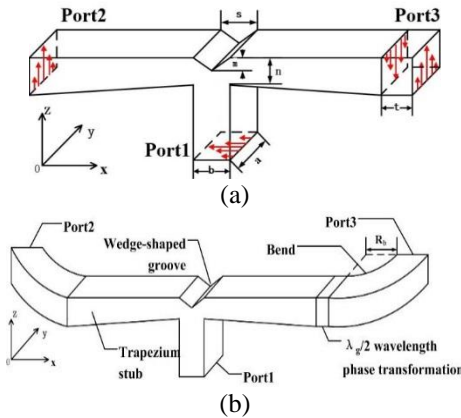


Fig. 1. Configuration of the E-plane T junction waveguide power divider: (a) $a=2.54$ mm, $b=1.27$ mm, $t=2.05$ mm, and (b) overall geometry ($R_b=2$ mm).

Table 1: The different structure of waveguide power divider

Index	Type		Graph
	Wedge Groove	Trapezoidal Port	
Case1	×	×	
Case2	×	√	
Case3	√	×	
Case4	√	√	

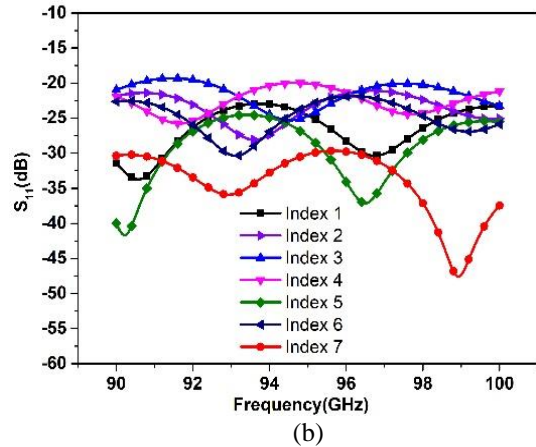
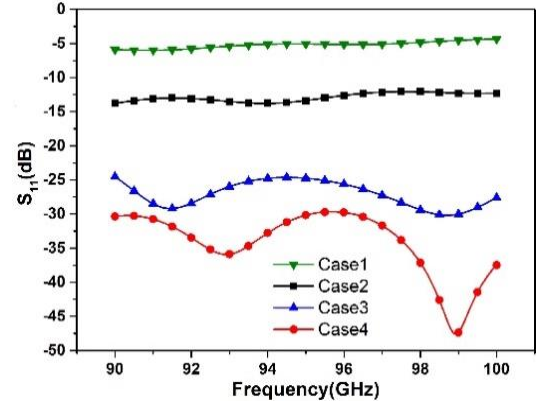


Fig. 2. Simulated S_{11} of the power dividers: (a) with different structure and (b) with different parameters.

The influence of the parameters of the wedge-shaped groove and the trapezium taper ports were studied by changing the values of s , m , and n . Figure 2 (b) illustrates the simulated S_{11} results of the antennas in case 4. We found that the performance of the waveguide was highly sensitive to changes in these parameters. The optimized parameters of the power divider are shown in Table 2, which were obtained by optimization using HFSS15.1 software. Clearly, the S_{11} curve represented by Index 7 is optimal at 94 GHz.

Table 2: The parameter scan




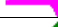


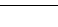
Index	Symbol	Parameter / mm		
		<i>s</i>	<i>m</i>	<i>n</i>
1		0.7	0.6	0.6
2		1.1	0.6	0.6
3		0.9	0.5	0.6
4		0.9	0.7	0.6
5		0.9	0.6	0.5
6		0.9	0.6	0.7
7		0.9	0.6	0.6

Figure 3 (a) gives the simulated S_{11} , S_{21} , S_{31} , and S_{23} of Fig. 1 (b). In the range of 90-100 GHz, S_{11} of our design was less than -30 dB, S_{23} was about -6 dB and its S_{21} and S_{31} were both at -3 dB. We found an excellent impedance matching and a good power allocation of the proposed power divider (Fig. 3 (a)). Figure 3 (b) shows the phases of port 2 and port 3. We found that they were nearly identical.

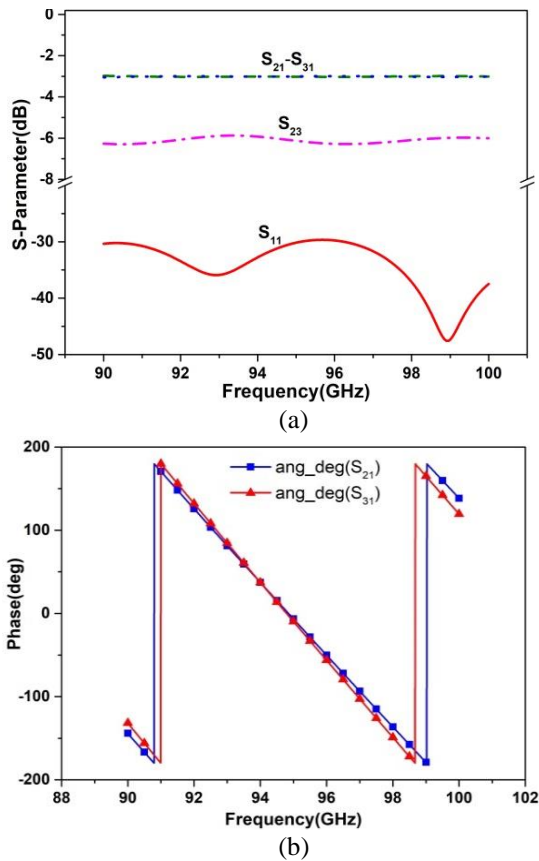


Fig. 3. Simulated results of T junction waveguide power divider: (a) S-parameters and (b) phase of the output ports.

The current distribution of the waveguide power divider is shown in Fig. 4. The wedge groove is used to realize the E-field transition between the output port

waveguide and the main waveguide and to maintain the uniform distribution of E-field in two trapezium taper ports.

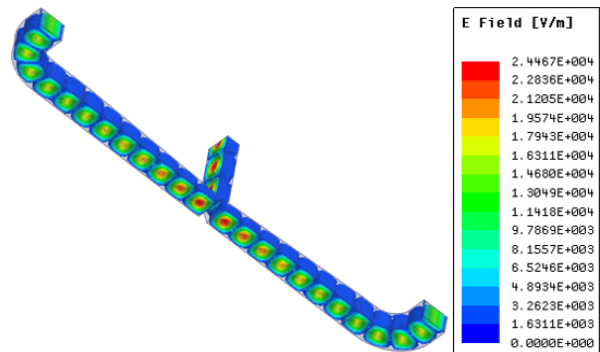


Fig. 4. Simulated E-field distribution at 94 GHz.

B. 94 GHz antenna design

The basic geometry of the proposed 94 GHz antenna is shown in Fig. 5. Its radiation characteristics are essentially a combination of the E- and H-plane sectorial horns. Figures 5 (a) and (b) show the xz-plane (H-plane) and the yz-plane (E-plane) of the pyramidal horn antenna, respectively. The optimal gain calculated for this horn antenna is proposed in [13]. The optimized parameters of the horn antenna can be obtained by:

$$A^4 - aA^3 + \frac{3bG\lambda^2}{8\pi\epsilon_{ap}}A = \frac{3G^2\lambda^4}{32\pi^2\epsilon_{ap}^2}, \quad (2)$$

and are listed in Table 3.

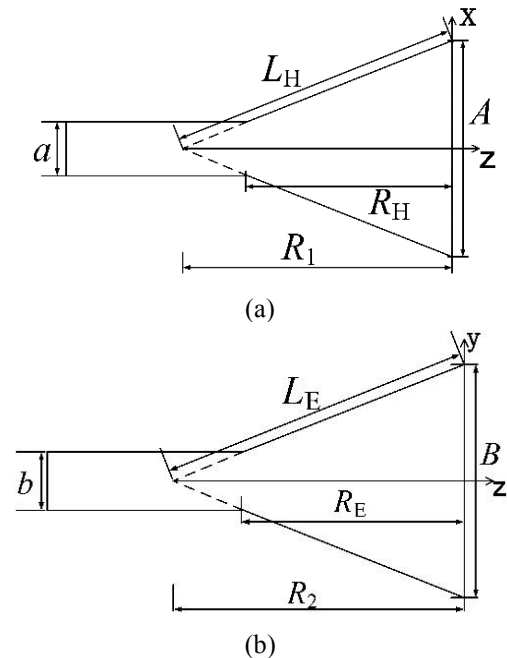


Fig. 5. The pyramidal horn antenna: (a) cross section of the xz-plane and (b) cross section of the yz-plane.

Table 3: Dimensions of the horn antenna

Parameter	Length/mm	Parameter	Length/mm
A	25.06	R_1	65.57
B	20.06	R_2	63.03
a	2.54	L_E	63.82
b	1.27	L_H	66.76
R_E	59.03	R_H	58.95

Figure 6 demonstrates the trend between radiation pattern and length. In order to achieve a >20 dB gain and >10° wider beam to improve the field of view (FOV), the length of the horn antenna was reduced. The length of R_H was 40 mm, while the gain was greater than 20 dBi and HPBW is 9.4° in the E-plane. However, the performance of a single antenna could not meet the design requirements, so a dual-pyramidal horn antenna with waveguide power divider was made.

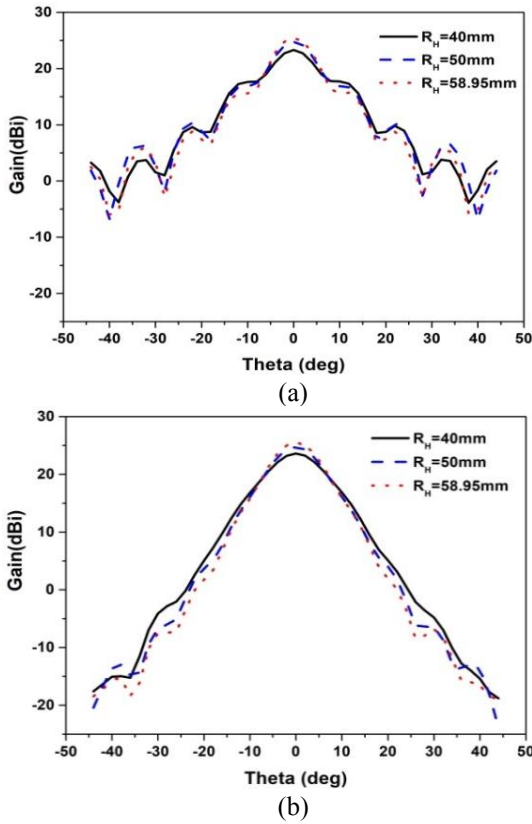


Fig. 6. The influence of length R_H on the proposed antenna: (a) E -plane and (b) H -plane.

The application of the antenna is shown in Fig. 7. H is the height of the antenna, and θ_{min} is the minimal degree in elevation. In the test environment, the height is fixed at a distance of 200 mm from the ground. According to the half power beam width of the antenna, the minimum detection range R_{min} of radar is estimated by:

$$R_{min} = H / \tan \theta_{min}. \quad (3)$$

A wider beam could improve the FOV. The maximum gain required by the radar prototype is greater than 20 dB, therefore reducing the length of the horn antenna would result in a reduction in gain, but we can achieve a smaller physical size, wider beam width and satisfactory gain.

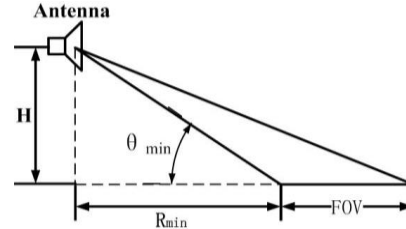


Fig. 7. Scenario for radar detection on the road.

C. Flange and overall structure

Figure 8 shows the 3D structural model of the proposed antenna. Considering that the interface of the radar machine is a wave port, we integrated the design of the antenna and the flange. The material used for the entire structure was *AlSi10Mg* and the model of the machine was a *SLM 125 Metal 3D Printer*. The type of flange was FUGP900. A 90° bend was used to connect the waveguide divider and the flange.

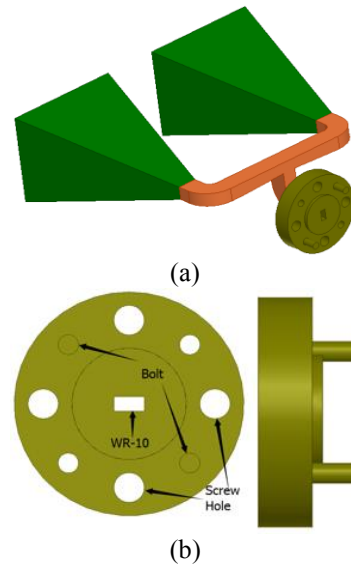


Fig. 8. 3D structure model of antenna: (a) overall structure and (b) flange.

III. EXPERIMENTAL RESULTS AND DISCUSSION

The proposed antenna was fabricated by 3D printing technology. Figure 9 shows the photographs of the fabricated antenna.

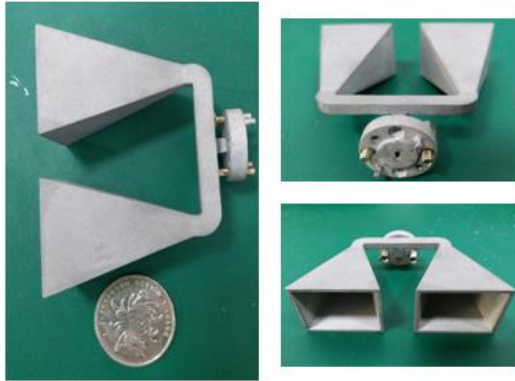


Fig. 9. Fabrication of the proposed antenna.

Figure 10 (a) shows the measured S_{11} of the proposed antenna. We found that the -10 dB impedance bandwidth of the proposed antenna was 3.3% (92.77-95.87 GHz). The antenna has another operating band of 3.4% (81.48-84.32 GHz), but this is not required. Figure 10 (b) shows the measured radiation pattern at 94 GHz. The data reveal that the peak gain of the antenna is higher than 21.2 dBi and the HPBW in E - and H -plane are 10.1° and 2.3° , respectively. The wider E -plane beam has advantages in obtaining higher azimuth resolution, while the narrower H -plane beam provides more accurate range resolution. All tests were performed in a microwave anechoic chamber.

As shown in Fig. 11 (a), the antenna was then assembled on a 94 GHz radar for application testing. A metal triangular trihedral corner reflector (TTCR) was used as a test target. The result of the test environment without TTCR is shown in Fig. 11 (b). It was placed at a distance from radar of both 6 m and 10 m. Figures 11 (c) and (d) show the normalized one-dimensional range profile of the reflector as measured by the radar. We found that although the ground clutter and other objects in the surrounding environment can create disruptive signals, an obvious peak can still indicate the detection of the target, providing evidence that our proposed antenna works on the 94 GHz radar.

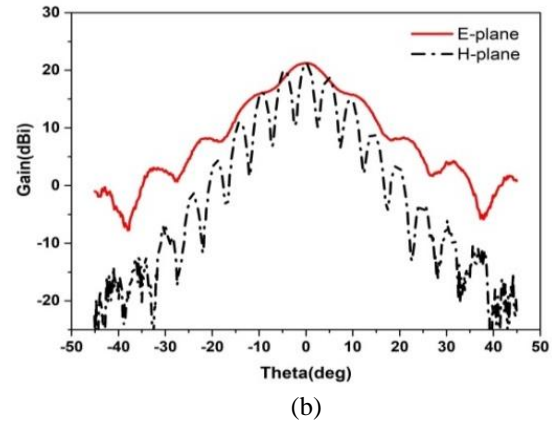
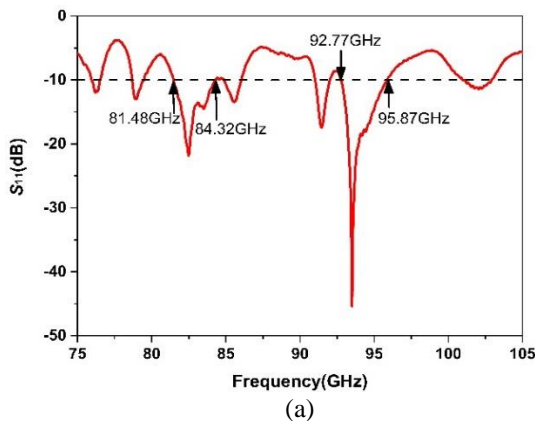
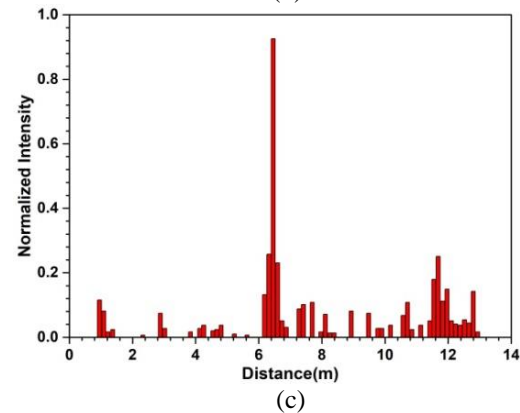
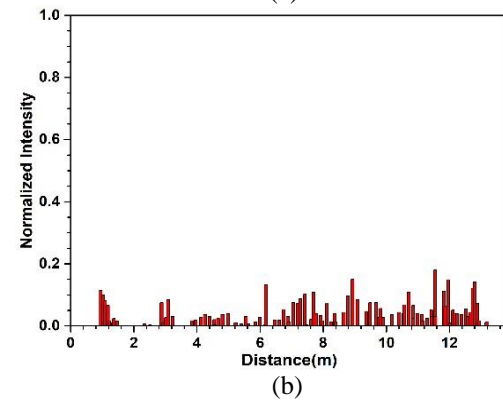
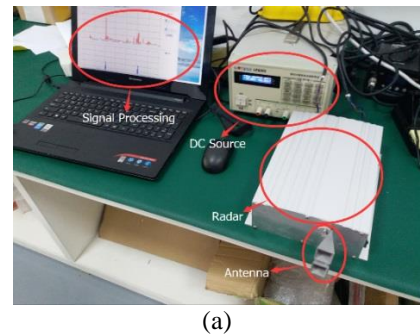


Fig. 10. Measured results of the antenna: (a) S_{11} of the proposed dual-horn antenna and (b) the radiation pattern at 94 GHz.



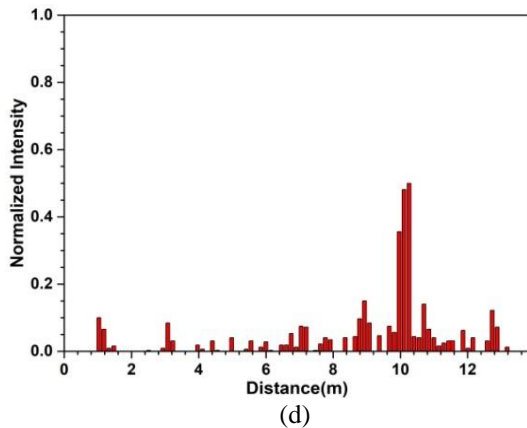


Fig. 11. Experimentally measured and normalized one-dimensional range profile of a metal TTCR. The experimental environment and background radiation measurement are shown in (a) and (b). Results at 6 m and 10 m are shown in (c) and (d).

IV. CONCLUSION

This paper describes the design and measurement of an improved waveguide power divider for dual-pyramidal horn antenna. The use of a waveguide power divider allowed for good impedance matching and matched phase for two output ports. The antenna showed characteristics of high gain, directivity, and a wide beam. The antenna structure created by 3D metal printing technology was strong and stable. A peak gain of 21.2 dBi and 10.1° beam in the E-plane was achieved. The performance of this design was also assessed in outdoor tests. We believe this design is an excellent fit for 94 GHz automotive application.

ACKNOWLEDGEMENT

The authors wish to acknowledge the support of the National Natural Science Foundation of China (Grants #61761017), Natural Science Foundation of Jiangxi Province (Grants #20192BAB207007), the Open Project of State Key Laboratory of Millimeter Wave (Grant #K201829) and Social science planning project of Jiangxi Province (Grant #17BJ40).

REFERENCES

- [1] F. Xu, X. Chen, and X. A. Wang, "K-band microstrip antenna array applied in anti-collision radar," *2010 IEEE 12th International Conference on Communication*, pp. 1240-1243, 2010.
- [2] J. Xu, W. Hong, H. Zhang, G. L. Wang, Y. R. Yu, and Z. H. Jiang, "An array antenna for both long and medium range 77GHz automotive radar application," *IEEE Transactions and Antennas Propagation*, vol. 65, no. 12, pp. 7207-7216, 2017.
- [3] Y. R. Yu, W. Hong, H. Zhang, J. Xu, and Z. H. Jiang, "Optimization and implementation of SIW slot array for both medium and long range 77GHz automotive radar application," *IEEE Transactions on Antennas and Propagation*, vol. 66, no. 7, pp. 3769-3774, 2018.
- [4] D. G. Macfarlane and D. A. Robertson, "A real time close range millimeter wave exhibition radar," *35th International Conference on Infrared, Millimeter, and Terahertz Waves*, pp. 1-2, 2010.
- [5] W. D. Hu, Y. Y. Zhao, H. Ren, J. J. Ji, M. D. Wu, and X. Lv, "Design and implementation of a 94GHz high resolution stepped frequency radar," *2016 IEEE International Conference on Microwave and Millimeter Wave Technology*, vol. 2, pp. 916-918, 2016.
- [6] Y. J. Cheng, Y. X. Guo, and Z. G. Liu, "W-band large-scale high-gain planar integrated antenna array," *IEEE Transactions on Antennas and Propagation*, vol. 62, no. 6, pp. 3370-3373, 2014.
- [7] Y. J. Cheng, W. Hong, and K. Wu, "94 GHz substrate integrated monopulse antenna array," *IEEE Transactions on Antennas and Propagation*, vol. 60, no. 1, pp. 121-129, 2012.
- [8] S. Ramesh and T. R. Rao, "High gain dielectric loaded exponentially tapered slot antenna based on substrate integrated waveguide for V-band wireless communications," *ACES Journal*, vol. 29, no. 11, pp. 870-880, 2014.
- [9] C. Migliaccio, J. Y. Dauvignac, L. Brochier, J. L. Le Sonn, and C. Pichot, "W-band high gain lens antenna for metrology and radar applications," *Electronics Letters*, vol. 40, pp. 1394-1396, 2004.
- [10] J. Wang, J. X. Ge, Y. Zhou, H. Xia, and X. Z. Yang, "Design of a high-isolation 35/94-GHz dual-frequency orthogonal-polarization cassegrain antenna," *IEEE Antennas and Wireless Propagation Letters*, vol. 16, pp. 1297-1300, 2017.
- [11] D. Sun and J. Xu, "Compact phase corrected H-plane horn antenna using slow-wave structures," *IEEE Antennas and Wireless Propagation Letters*, vol. 16, pp. 1032-1035, 2017.
- [12] Y. Wu, B. Zhang, K. Ding, and R. Li, "A metallic 3D printed K-band ridged horn antenna," *ACES Conference: Advanced Manufacturing Technologies for Microwave Devices*, 2017.
- [13] H. B. Zhan, Y. Li, Y. C. Zuo, Q. L. Hu, and Y. H. Wang, "A 10-100-GHz double-ridged horn antenna and coax launcher," *IEEE Transactions on Antennas and Propagation*, vol. 63, pp. 3417-3422, 2015.
- [14] D. H. Park, "Design of millimeter-wave monopole Yagi-Uda-Fed waveguide pyramidal horn antennas," *International Conference on Platform Technology and Service*, pp. 1-5, 2017.
- [15] Y. C. Ou and G. M. Rebeiz, "On-chip slot-ring and high-gain horn antennas for millimeter-wave wafer-scale silicon systems," *IEEE Transactions*

on *Microwave Theory and Techniques*, vol. 59, pp. 1963-1972, 2011.

- [16] T. Sehm, A. Lehto, and A. V. Raisanen, "A large planar 39-GHz antenna array of waveguide-fed horns," *IEEE Transactions on Antennas and Propagation*, vol. 46, pp. 1189-1193, 1998.
- [17] K. C. Hwang, "Design and optimization of a broadband waveguide magic-T using a stepped conducting cone," *IEEE Microwave and Wireless Components Letters*, vol. 19, pp. 539-541, 2009.
- [18] P. Zhao, Q. Y. Wang, F. Zhang, and X. He, "An integratable planar waveguide power divider with anti-phases and full bandwidth," *IEEE Microwave and Wireless Components Letters*, vol. 26, pp. 583-585, 2018.
- [19] S. Y. Hu, K. J. Song, F. Zhang, Y. Zhu, and Y. Fan, "A novel compact wideband four-way W-band waveguide power divider with low insertion loss," *2016 IEEE MTT-S International Microwave Workshop Series on Advanced Materials and Processes for RF and THz Applications*, pp. 1-3, 2016.
- [20] W. J. Feng, W. Q. Che, and K. Deng, "Compact planar magic-T using E-plane substrate integrated waveguide (SIW) power divider and slotline transition," *IEEE Microwave and Wireless Components Letters*, vol. 20, pp. 1-3, 2010.



Xianyan Zhang received the B.S. degree in Applied Physics and M.S. degree in Physical Electronics from Yunnan University, Kunming, China, in 2001 and 2004 respectively, and the Ph.D. degree in Electromagnetic Field and Microwave Technology from Institute of Electronics, Chinese Academy of Sciences in 2007. Her research interests include electromagnetic computation, antenna design and wireless power transmission structure design.



Yuting Chen received the B.S. degree in School of Information Engineering from East China Jiaotong University, Nanchang, China, in 2013, and the M.S. degree in Information and Communication Engineering from East China Jiaotong University, Nanchang, China, in 2019. His research interests include electromagnetic band-gap structure, antenna design.



Yan Xie was born in Nanchang, Jiangxi, China in 1987. He received the B.S. degree in Electronic Information Engineering and M.S. degree in Signal and Information Processing and the Ph.D. degree in Electromagnetic Field and Microwave Technology from Beijing University of Aeronautics and Astronautics, Beijing, China, in 2007, 2010, and 2014, respectively. His research interests include the development of microwave and millimeter wave system, radio frequency circuit and algorithm simulation.



Lingfeng Liu received his B.S. degree in Electronic Information Engineering from Wuhan University, China, in 2005, his M.S. degree in Signal and Information Processing in Communications from Aalborg University, Denmark, in 2007, and his Ph.D. degree in Electrical Engineering from the Universite Catholique de Louvain (UCL) and the Universite Libre de Bruxelles (ULB), Belgium, in 2012. From 2007 to 2012 he was a Research Assistant at ICTTEAM Electrical Engineering (UCL). Since 2012, he has been working as a Lecturer and later Associate Professor at the School of Information Engineering of the East China Jiaotong University, China. His research interests cover channel characterization and modeling in body area networks, MIMO channel estimation and modeling, and cooperative communication networks.